



Towards heterogeneous integration of optical isolators and circulators with lasers on silicon [Invited]

DUANNI HUANG,* PAOLO PINTUS, AND JOHN E. BOWERS

Department of Electrical and Computer Engineering, University of California Santa Barbara, Santa Barbara, CA 93106, USA

*duanni@umail.ucsb.edu

Abstract: Optical isolators and circulators are extremely valuable components to have in photonic integrated circuits, but their integration with lasers poses significant design and fabrication challenges. These challenges largely stem from the incompatibility of magneto-optic material with the silicon or III-V platforms commonly used today for photonic integration. Heterogeneous integration using wafer bonding can overcome many of these challenges, and provides a promising path towards integrating isolators with lasers on the same silicon chip. An optical isolator operating for TE mode with 25 dB of isolation, 6.5 dB of insertion loss, and tunability over 40nm is demonstrated and a path towards integrating this isolator with the heterogeneous silicon/III-V laser is described.

© 2018 Optical Society of America under the terms of the [OSA Open Access Publishing Agreement](#)

1. Introduction

Rapid development in photonic integrated circuit (PIC) technology using silicon waveguides has been made possible by an increasingly advanced library of photonic elements. By utilizing high quality silicon on insulator (SOI) wafers and borrowing decades of CMOS processing expertise, researchers have demonstrated low-loss waveguides, modulators, and photodetectors [1]. These elements serve as building blocks for complex silicon photonic systems on chip for applications such as sensing [2,3], interconnects [4,5], and quantum optics [6]. In most of these works, an external laser is used with a bulk optical isolator, which limits the size, power consumption, and cost of the product. The isolator is needed to block reflections from the PIC, such as those caused by the edge or grating coupler, from reaching the laser. A fully integrated solution in which the laser and isolator are on the same silicon chip has not realized to date. Since silicon does not emit light efficiently due to its indirect bandgap, Ge or III-V materials are required for electrically pumped lasers on silicon [7,8]. One way to introduce III-V material into silicon photonics is through wafer bonding processes [9]. This approach, termed “heterogeneous” integration, can be used to bond III-V material directly on top of the silicon chip prior to laser fabrication. This approach has tremendous benefit due to precise lithographic alignment between III-V and silicon, as well as increased scalability when compared to attaching pre-fabricated III-V chips to silicon dies [10]. Since the first heterogeneous silicon laser was reported over a decade ago [11], increasingly complex PIC containing hundreds of elements have been demonstrated using heterogeneous integration for transceivers, interconnects as well as sensing applications [12–15]. The technology has recently reached commercialization [16].

Despite the increasing maturity and complexity of heterogeneous silicon photonics, the lack of a readily available on-chip optical isolator limits the performance of these PICs, especially given the often-strict performance requirements for the integrated laser. Ideally, the isolator should be placed directly after the laser, to minimize the effect of undesired reflections from the rest of the PIC. Integrated circulators can separate counter-propagating light waves and can give rise to bidirectional transmission and optical amplification [17]. Inclusion of isolators and circulators in the heterogeneous silicon photonic library is highly desirable, and crucial for some applications. The same wafer bonding technology used to

realize lasers on silicon can be extended to bond magneto-optic materials for optical isolators and circulators. This highlights the ability to take the best material for each function, and heterogeneously integrate them together using silicon waveguides as a common denominator [15]. This flexibility will give rise to multi-functional, high performance PIC, since compromises do not need to be made from a material standpoint. This paper addresses the challenges and solutions associated with such an approach.

This paper is organized as follows. First, we provide a brief overview of integrated optical isolators and circulators, their operating principles, and notable demonstrations to date. Then, we discuss the requirements and challenges associated with integrating such isolators with heterogeneous silicon/III-V active devices such as lasers, modulators, and photodiodes. Finally, we present our progress in this area, and demonstrate a widely tunable microring based optical isolator operating for transverse electric (TE) polarization.

2. Overview of integrated isolators and circulators

Optical isolators and circulators are nonreciprocal components. They are characterized by allowing the propagation of light in one specific direction, such that their scattering matrix is non-symmetric [18]. The device symmetry can be effectively broken in three different ways: i) by spatiotemporal modulation (STM) of the refractive index; ii) exploiting nonlinear effects (NLE) and iii) using magneto-optical (MO) materials.

In STM case, the nonreciprocity of the device is induced by modulating the refractive index of the waveguide, usually with a microwave [19] or acoustic signal [20]. For a given propagation direction, the modulating signal is used to couple the incident light with different modes or frequencies that can be filtered or radiated out of the device [21]. This modulating signal has no effect on counter-propagating light. Integrated optical isolators have been demonstrated exploiting the electro-optic effects in a travelling wave III-V modulator [22] as well as a tandem phase modulator [23]. Similar isolators were achieved in silicon [19,24]. No additional materials are needed, making STM based isolators very attractive for integration with lasers. However, the operation of the isolators often requires complex, high-speed drive circuits that can consume large amounts of power.

In the second approach, a NLE is tailored to achieve nonreciprocal behavior. However, not all nonlinear effects can be used for this purpose, as some effects such as Kerr-like nonlinearities are subject to dynamic reciprocity [25]. When a forward and backward propagating signal are simultaneously propagating through the device, the nonreciprocity of the system can break down, and the device cannot be used to perform isolation. Nonlinear effects suitable for isolation are Raman amplification [26], stimulated Brillouin scattering [27], and parametric amplification [28] among others. Like STM based isolators, the NLE isolators do not require materials outside of those commonly found in CMOS or III-V based foundries. However, a drawback of using nonlinear effects is the inherent dependence between optical isolation of the device and the optical power of the incident light. This is undesirable as the feedback to the laser should be minimized regardless of the output power. Furthermore, they also suffer from small isolation bandwidths since they generally rely on phase matching, meaning isolation is only performed at a specific wavelength.

The last approach uses MO material to break the reciprocity of the system when immersed in a magnetic field. If the light is propagating in the same direction of the external applied magnetic field as in Fig. 1(a), the plane of polarization rotates, otherwise known as Faraday rotation. This approach is widely used in free-space optical isolators, but challenging to implement in waveguides, which are highly birefringent [29,30]. To overcome this, quasi-phase matched approaches by periodically modulating the Faraday rotation along the length of a waveguide have been demonstrated [31,32]. However, a drawback of these devices is the need for polarization manipulating components before and after the Faraday rotator, such as a 45-degree polarization rotator [33]. These components are harder to implement in integrated optics compared to their bulk counterparts.

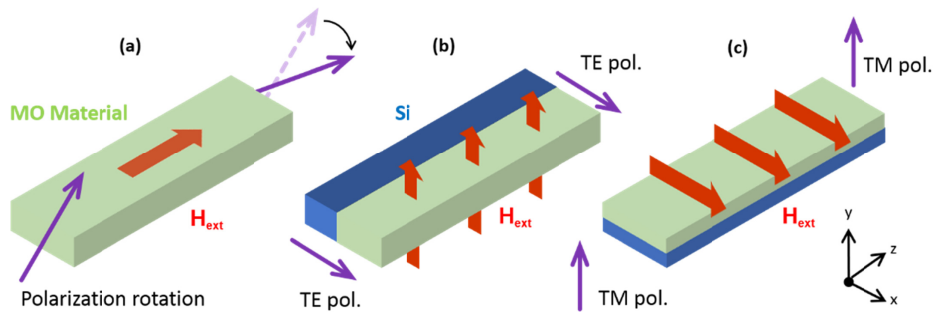


Fig. 1. Schematic of the various magneto-optic effects used to realize optical nonreciprocity for light propagating in the z -axis (a). Faraday rotation occurs when $\mathbf{H}_{z,\text{ext}} \neq 0$, resulting in polarization rotation. When (b) $\mathbf{H}_{y,\text{ext}} \neq 0$ or (c) $\mathbf{H}_{x,\text{ext}} \neq 0$, NRPS is present, and maximized for TE and TM modes respectively for the depicted waveguide geometries.

When the magnetic field is perpendicular to the direction of propagation, the light shows nonreciprocal phase shift (NRPS) and nonreciprocal loss (NRL) between the forward and backward directions. Isolators based on NRL have been realized by coating the sidewall [34] or top surface [35] of a waveguide with magnetic material such as iron. To compensate the large optical losses induced by the magnetic material, the waveguide should serve as a semiconductor amplifier (SOA). While NRL isolators have been integrated with lasers [36], it comes at the cost of high power consumption, large optical loss, and additional noise generated by the SOA. Even for large SOA drive current ($I = 150$ mA), the optical losses (14.1 dB/mm) are on the order of the isolation ratio (14.7 dB/mm) [34]. There is an inherent tradeoff between optical isolation and insertion loss.

On the other hand, the NRPS effect is purely passive so that it does not introduce additional noise or loss. The light exhibits a direction dependent phase velocity such that properly designed interferometric devices such as ring resonators [37–40], Mach-Zehnder interferometers (MZI) [41,42], multimode interferometers (MMI) [43], and photonic crystals [44] can generate constructive interference for forward light and destructive interference for backward light. To date, the best isolator and circulator performance in terms of lowest insertion loss (2.3 dB) [40], highest optical isolation (33 dB) [45], and largest isolation bandwidth (>20 dB over 18 nm) [46], are all based on NRPS. Since the NRPS effect is sensitive to the light polarization, the waveguide must be designed accordingly. The waveguide cross-section and the external magnetic field required for maximizing the NRPS effect for the transverse electric (TE) and transverse magnetic (TM) mode are shown in Fig. 1(b) and 1(c), respectively. The waveguide cross-section is discontinuous along the polarization direction, while the external magnetic field is perpendicular with respect to it [47].

The typical MO material for NRPS based waveguides at the telecom wavelengths is yttrium iron garnet (YIG), for which the yttrium atom can be substituted with cerium or bismuth to form Ce:YIG and Bi:YIG respectively to increase Faraday rotation. Significant efforts have been taken to deposit Ce:YIG on silicon using pulsed laser deposition [39] or sputtering techniques [48]. This is especially challenging due to the large thermal and lattice mismatch between silicon and YIG. One solution uses a YIG seed layer to promote crystallization of the Ce:YIG into the proper phases, which achieved a Faraday rotation of 3000 deg/cm [49]. More recently, a cerium substituted terbium iron garnet (Ce:TIG) with 3274 deg/cm has been deposited on silicon without a seed layer, which could simplify the deposition process and increase NRPS [50]. Both techniques result in polycrystalline garnet films, due to the lack of lattice matching. When Ce:YIG is instead grown on its native, lattice matched gadolinium gallium garnet (GGG) substrate, the Faraday rotation can be as high as

4500 deg/cm [51]. While monolithic garnet approaches continue to develop at a rapid rate, a heterogeneous approach in which the Ce:YIG is first grown on native substrate, and then bonded onto silicon has shown the best results to date [52]. Furthermore, heterogeneous integration of the garnet may be more suitable for laser integration from a design and fabrication standpoint, as we will discuss in the following sections.

3. Laser integration challenges and solutions

This section covers the requirements and challenges associated with integrating an optical isolator with a laser source on the same chip. The focus will be on heterogeneous integration on silicon, although many of the same arguments carry over to III-V PICs.

3.1 Integration with a heterogeneous silicon/III-V laser

The optical isolator should be placed directly after the laser for optimal performance. Thus, the process flow for the isolator and laser must be compatible with each other. From a fabrication standpoint, the challenges lie in managing the thermal budget of the process, as well as the simultaneous processing of vastly dissimilar materials (III-V, silicon, and garnet). While the lattice constant mismatch can be somewhat alleviated by wafer bonding, the thermal expansion coefficient mismatch between III-V and silicon provides a limited thermal budget for the process. Rapid thermal anneal performed at 420C for 2 minutes have degraded laser performance [53], and temperatures should be ideally kept below 300C. Monolithic approaches for garnet deposition may have a difficult time meeting this thermal budget. Studies have shown that 650C is required to crystallize YIG [54], and TIG films are annealed even hotter, at 900C [55]. Therefore, if a monolithic approach is pursued, the garnet would have to be deposited near the beginning of the process, prior to any III-V bonding to preserve the thermal budget for the rest of the process. This could affect subsequent steps and may require a complete retooling of the heterogeneous silicon/III-V process. Alternatively, bonding of garnet is attractive as it can be added as a back-end process after laser fabrication. Since the garnet is already fully crystallized prior to bonding, the thermal anneal is not required. In fact, the highest temperature process in isolator fabrication is 200C [40], which will not negatively impact the laser performance. The inclusion of the isolator processing at the end also reduces the amount of overlap with laser fabrication, which simplifies the process greatly.

From a design standpoint, one of the main challenges is the mismatch of waveguide dimensions between the laser and the isolator. The cross-section of the heterogeneous silicon/III-V laser is shown in Fig. 2(a). It has a silicon waveguide height of 500nm, which is chosen to match the refractive index of the silicon slab with the thick InP gain region. Silicon waveguides thinner than 400nm will suffer from low coupling to the InP [56]. However, the optimal silicon thickness for isolators is between 200 and 250nm, as seen in Fig. 2(b). It is possible to transition between the two silicon waveguides using a partial etch and taper structure [57], but this roughens the silicon surface, which complicates the bonding process. Furthermore, the taper could serve as a source of reflections. Since the main purpose of the isolator is to block reflections from reaching the laser, the isolator should not introduce significant reflection. A potential solution may be the local oxidation of silicon [59], which thins down a lithographically defined area of the wafer. Although this would be performed at the beginning of the process, prior to waveguide etching, it preserves the smooth surface for bonding III-V and MO material. Other design challenges are matching the operating polarization of the isolator with the laser, as well as biasing a magnetic field across the device in an efficient, compact, and integration friendly manner. These are further explored in the following sections.

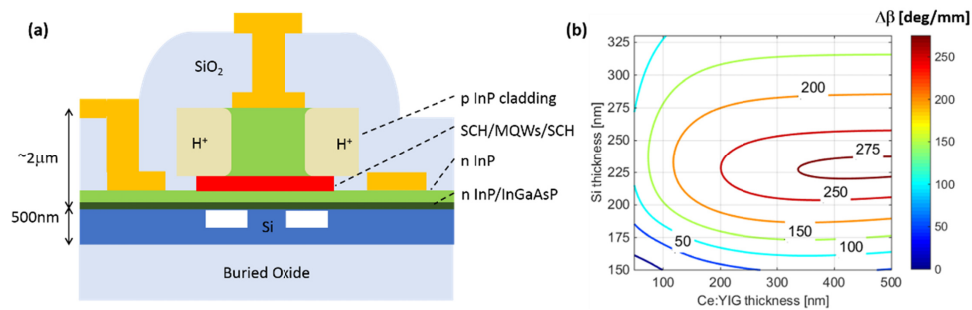


Fig. 2. (a) Schematic of the typical heterogeneous silicon/III-V laser structure formed by direct wafer bonding. (b) The optimal Si and Ce:YIG thicknesses to maximize the NRPS for a 600nm wide waveguide [58].

3.2 Polarization

Most semiconductor lasers output in TE polarization, so an optical isolator should also operate for TE polarization or be polarization independent. However, the NRPS effect is polarization dependent, as previously discussed. For the NRPS to be maximized for the TE polarization, the garnet should be placed on the side of the waveguide, rather than on top as in the case of wafer bonding. Clearly, this is a waveguide geometry more suitable for monolithic garnet integration rather than the heterogeneous approach. While NRPS for TE mode has been demonstrated using amorphous silicon waveguide on garnet substrates [60], it remains a challenge for the more commonly used SOI platform.

It has been proposed that the garnet can be deposited in a trench adjacent to a silicon or silicon nitride waveguide [47], for which the dimensions can be optimized to maximize the NRPS. However, fabrication of these structures remains a challenge due to high aspect ratio of the trench. A better approach may be to deposit only on one sidewall of the waveguide [61], while protecting the other sidewall with silicon dioxide cladding. For either approach, the magnetic field direction needed to maximize NRPS for TE modal geometry is out-of-plane. For Ce:YIG, this is the hard axis of magnetization, meaning that strong magnetic fields ($>2\text{kOe}$) would be required to observe NRPS, as opposed to the weak ($\sim 50\text{ Oe}$) magnetic fields needed to magnetize the easy axis [54]. Overall, while a monolithic approach is very attractive, the challenges discussed here as well as the thermal budget concerns limit its practicality for now.

Alternatively, TM-mode isolators have been integrated with TE \rightarrow TM polarization rotators before the isolator [62,63]. This effectively changes to operating polarization of the isolator to TE mode, provided the polarization extinction ratio (PER) is comparable to the isolation. Polarization rotators for silicon photonics have been widely studied and characterized, and a review of such technologies is covered in [64]. The polarization rotator should have low insertion loss, small back-reflection, broadband operation, and ideally be tolerant in fabrication variation. The polarization splitter rotator (PSR) satisfies all these requirements and has been demonstrated using a variety of designs on silicon [65]. The PSR comprises of two components. The first is a mode converter that converts couples the TE₀ and TE₁ modes together. This is a common component in mode-multiplexed systems and can be achieved using asymmetric directional couplers [66], multimode interferometers (MMIs) [67], or an adiabatically tapered coupler [68]. The second portion of the rotator consists of a linear taper to convert the TE₁ into the TM₀ mode. Mode hybridization can occur between the TE₁ and TM₀ modes at a certain waveguide width, provided there is a break in the vertical symmetry of the waveguide. Here, it is possible to utilize the bonded garnet upper cladding of the waveguide to realize such an effect.

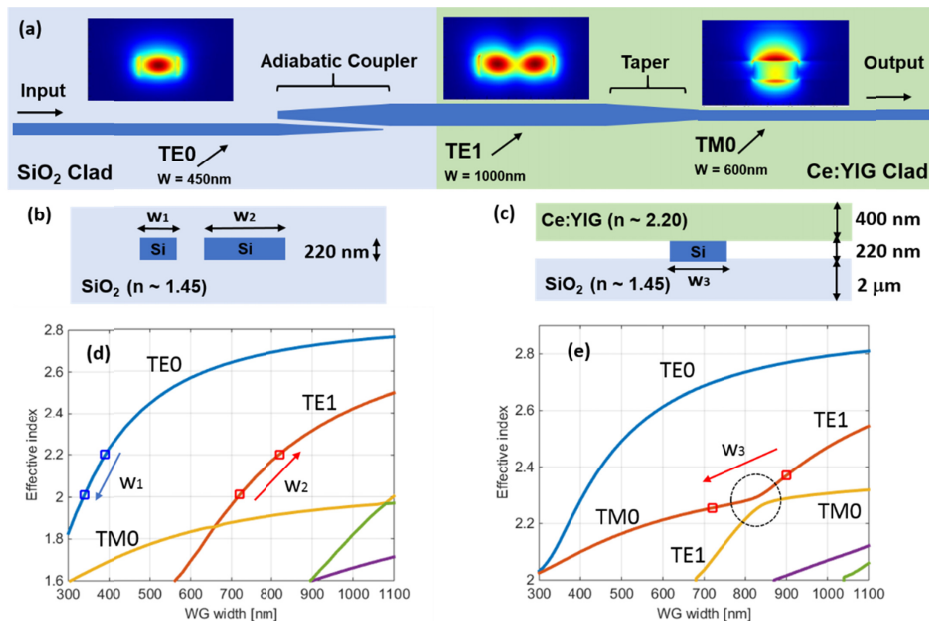


Fig. 3. (a) Schematic of the TE/TM polarization rotator consisting of an (b) adiabatic coupler and (c) linear taper under the Ce:YIG region. If the widths and lengths of the coupler (d) and taper (e) are chosen according, the transition can be fully adiabatic, resulting in efficient, broadband polarization rotation.

The details of the PSR are shown in Figs. 3(a)-3(e). It consists of an adiabatically tapered coupler (100 μm long) for $\text{TE0} \rightarrow \text{TE1}$ mode conversion, followed by a linear taper (150 μm long) to convert from $\text{TE1} \rightarrow \text{TM0}$. If all components of the rotator are adiabatically designed, the polarization rotator can be broadband. Furthermore, the advantage of this polarization rotator over previous TM mode isolator plus TE/TM rotator devices is improved fabrication tolerance [63] as it does not require electron-beam lithography, and fabrication simplicity [58] since it does not require any additional processing steps such as a polysilicon or silicon nitride overlay on the waveguide.

3.3 Applying a magnetic field

The operation of a MO based isolator requires a magnetic field. Traditionally, an external magnet is packaged with the isolator to provide a static magnetic field. This is undesirable for an integrated isolator, as the magnet adds significant bulk and creates challenges for packaging. It has been shown that latching thin-film garnets can be achieved by incorporating europium during growth to lower the saturation point, offering magnet-free operation [69]. However, the magnetization direction is out-of-plane, and therefore the film must be flipped to be perpendicular to light propagation [70]. This approach has drawbacks when considering the planar nature of waveguides in PIC, as it can only be placed on the edge of the chip or placed in grooves that are pre-etched into the chip.

One solution is to fabricate an electromagnet directly on chip. In addition to reducing the footprint of the device, the electromagnet provides a variable magnetic field strength and thermal tuning. This flexibility is extremely important for an integrated device, as it can account for fabrication imperfections or material variability. For example, the magnetic field can be tuned to be slightly stronger if the Faraday rotation of the garnet is weaker than expected. Furthermore, some isolator geometries such as the microring isolator require a radially orientated magnetic field, which is difficult to achieve with external magnets without compromising the size of the ring [38] or sacrificing overlap between the garnet and the resonator [39].

For an NRPS based optical isolator, the magnetic field must be transverse to the waveguide, so the electromagnet should be placed on top of the waveguide, as shown in Fig. 4(a). Since magnetic field strength decays with distance, it is important to place the electromagnet near the waveguide core. This is also crucial since power dissipation in the electromagnet scales quadratically with the distance to the waveguide. For the heterogeneous process, this waveguide to electromagnet distance is minimized by removing the substrate of the bonded garnet, often using a mechanical polishing technique. A multicoil geometry for the electromagnet can also be adopted to reduce the drive current [71]. While this does not reduce the power consumption, it reduces the current density in the electromagnet, which is important for avoiding electromigration based failure mechanisms [72]. The combined effects of the multicoil electromagnet and thinner garnet substrate result in significant improvement in terms of the efficiency of the magnet. For a 1 mm long waveguide with the cross-section shown in Fig. 4(b), only 27 mA of current is needed to obtain a phase shift $\Delta\phi$ of 180 degrees between forward and backward propagating light. The NRPS saturates at a value of $\Delta\beta = 270$ deg/mm, which is in good agreement with the predicted value in Fig. 2(b). For a push-pull configuration commonly used in MZI, $\Delta\phi = 90$ degrees is needed per arm, such that only 13.5 mA and current and 3.6 mW of power is consumed, given the 20 Ohm resistance in the electromagnet.

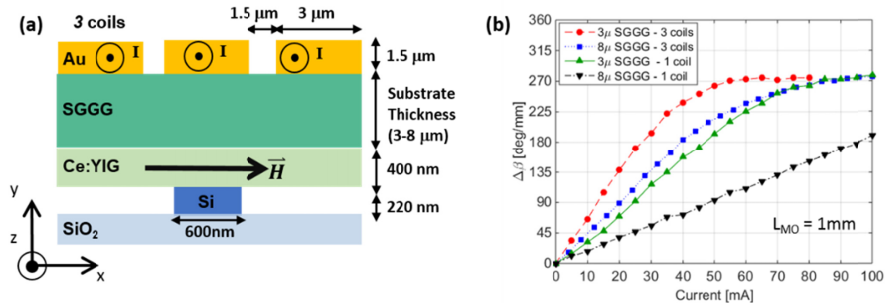


Fig. 4. (a) Cross sectional schematic of the Si waveguide with the bonded Ce:YIG and integrated electromagnet. Multiple narrowly spaced coils of the electromagnet increase the magnetic field strength at the waveguide and results in larger NRPS for a given current. (b) Experimental data showing the increase in NRPS for thinner SGGG and multi-coils. Adding too many coils provides diminishing returns, as the outer coils do not contribute as much to the transverse magnetic field. NRPS increases linearly until the magnetization in the material is saturated.

Further improvements can be made in the substrate removal process. With dynamic levelling of the wafer, substrate thickness as thin as 1 micron should be achievable. A chemical substrate removal process is advantageous for increased uniformity and repeatability but may be difficult to implement for garnets without a dedicated etch stop layer. An alternate method for substrate removal could be “smart cut” [73], in which a defect layer is planted in the garnet using heavy ion implantation, and then released using thermal or chemical treatment [29]. If this implantation is done prior to bonding, then a thin film of garnet could be transferred to silicon following wafer bonding and subsequent release process. Thus, ion implantation should be deep enough to avoid roughening the surface prior to bonding, but not so deep as to increase the distance to the waveguide too much. The film release can also be done prior to bonding, but the handling of such a thin, brittle garnet film poses a challenge [74]. For monolithic processes where the garnet is deposited instead of bonded, the fabrication could be further simplified, as the distance between the waveguide and electromagnet can be precisely controlled during cladding deposition.

The last approach uses a planar thin-film permanent magnet that is deposited on top of the garnet. While Ce:YIG has possess ferromagnetic properties, its remnant magnetization for the easy axis is fairly weak [75], and is prone to being demagnetized. Instead, it is possible to

deposit a material with high magnetization and coercivity such as samarium cobalt on the backside of the garnet [76]. A spacer layer such as silica is needed to avoid optical losses in the thin-film magnet. This film can be magnetized locally using an on-chip electromagnet, which allows for more versatile geometries. Ideally, only a short pulse of current is needed to magnetize the thin film, after which it retains the field [77]. This approach is attractive since it maintains a small form factor, while eliminating any steady state power consumption in the isolator. Further studies should be performed to determine reliability and sensitivity to demagnetization of such an approach.

4. Heterogeneously integrated optical isolator for the TE mode

Taking the design considerations of the previous section into account, a widely tunable integrated microring optical isolator operating for TE mode is presented. This is the first microring based isolator operating for TE mode to the best of our knowledge. A microscope image of the isolator is shown in Fig. 5(a), in which a 3-coil Archimedean spiral is used for the electromagnet. The cross-section of the ring resonator is identical to the one shown in Fig. 4(a). The TE→TM polarization rotator described in the previous section is integrated right before the isolator. A TM→TE rotator could also be placed after the isolator, but is not done here in order to characterize the insertion loss and PER of a single polarization rotator.

The transmission spectrum is measured with a tunable laser sweep and shown in Fig. 5(b). First, the performance of the polarization rotator is characterized by comparing the spectrum through the ring isolator plus rotator (TE input) with the spectrum through a reference Si/Ce:YIG waveguide (TM input) of the same geometry. The polarization rotator introduces 0.8 dB of insertion loss at 1550 nm, and <2 dB of loss across the whole wavelength range of 1520 nm to 1580 nm. The PER of the rotator is measured by adding a polarizer at the output of the isolator and measuring the residual TE light in the waveguide. The PER near 1550 nm is 25 dB, and ranges from 20 dB to 30 dB across the whole wavelength range. The broadband characteristics of the polarization rotator is attributed to the adiabatic design. The total insertion loss of the isolator is 6.5 dB compared to a Si only waveguide (TE input) at 1550 nm. The primary contributions to the loss is caused by the Ce:YIG upper cladding as well as the transition into the bonded Ce:YIG region. This can be further reduced by shortening the length of the Si/Ce:YIG bus waveguide, which is 2 mm long in this case. The isolation ratio is measured by injecting TE polarized light into the device while sweeping the current applied to the electromagnet. Flipping the orientation of the current is identical to changing the propagation direction of light. A split in the resonant wavelength between forward and backward propagation is observed for 40 mA of current, which results in a maximum of 25 dB optical isolation as shown in Fig. 5(c).

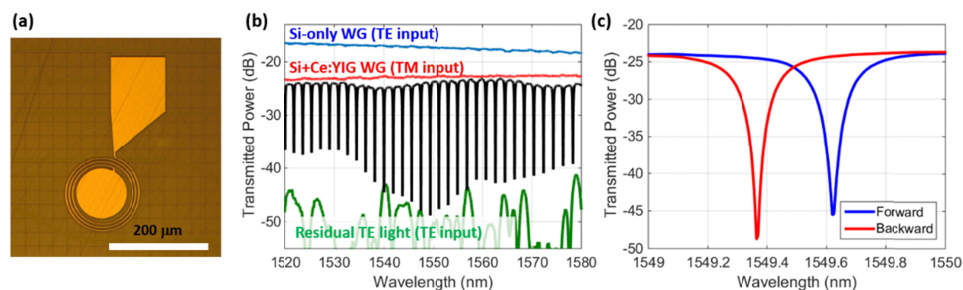


Fig. 5. (a) Microscope image of the microring isolator with TE/TM rotator (not shown). (b) The measured transmission spectra of the isolator with no applied current is shown in black, and compared to reference waveguides. (c) The transmission spectra of the isolator at 1549.5 nm for 40 mA of applied current showing 25 dB of optical isolation.

The isolation bandwidth is shown in Fig. 6(a). For a single ring isolator, the 20dB isolation bandwidth is 2.8 GHz. Cascading two or more ring isolators together can further

increase this bandwidth [71]. If a MZI structure is used instead of a ring, the isolation bandwidth can be as large as 18 nm, at the cost of larger footprint, insertion loss, and power consumption [46]. For MZI devices operating for TE mode, the polarization rotator must be broadband otherwise the isolation ratio will be limited by the PER. A ring isolator should be tunable in order to match the operating wavelength of the laser in a PIC. The Joule heating in the electromagnet can be used here to align the isolation wavelength, as shown in Fig. 6(b). The blue line depicts the MO nonreciprocal wavelength split, while the red line is the shift in resonance wavelength due to Joule heating. The MO effect saturates as the magnetization is saturated, and then slightly decreases at higher currents due to heating. Both mechanisms affect the isolation wavelength, which is plotted as a function of applied current (clockwise and counterclockwise injection) in Fig. 6(c). The isolation wavelength can be tuned across a full free spectral range (FSR) of the ring, meaning the isolator is widely tunable. A variety of techniques can be used to lock the isolator to the laser wavelength once it is aligned [78]. Over 20 dB of optical isolation can be achieved anywhere from 1540 nm to 1580 nm with proper tuning, as depicted for few select wavelengths in Fig. 6(d). The limitations of the range stem from the deviation of the ring from its critical coupling state, which provides the largest extinction ratio. The bandwidth of the polarization rotator could also limit the tuning range, but is not a concern for this device.

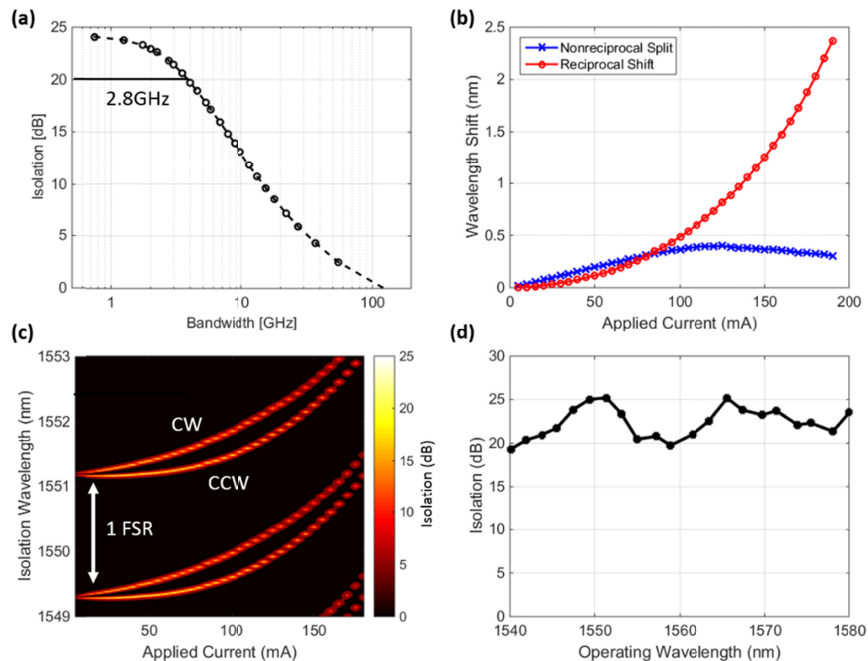


Fig. 6. (a) Optical bandwidth of the isolator for different isolation levels. (b) The thermal (reciprocal) and MO (nonreciprocal) induced shifts on resonance wavelength with respect to applied current. Both effects can be used to tune the wavelength a full FSR in (c) while maintaining high isolation ratio. (d) The tuning allows for larger than 20 dB of optical isolation anywhere from 1540 nm to 1580 nm.

5. Conclusions

In conclusion, a path towards heterogeneous integration of isolators and circulators with lasers on silicon has been presented. While monolithic approaches to integrate MO garnet on silicon continue to develop at a rapid rate, they require a high temperature anneal, which is incompatible with back-end processing. Heterogeneous integration of the garnet after the laser is processed provides a very promising solution, provided the polarization mismatch is

addressed. A broadband polarization rotator with low loss is demonstrated with no additional fabrication steps. For a fully integrated laser with isolator, the magnetic field source should also be integrated on-chip. Here, an integrated electromagnet is utilized, which provides a greatly needed tuning mechanism for the isolator when considering PIC operation. Proper design of the electromagnet can significantly reduce the current and power consumption. A widely tunable microring isolator operating for TE mode with 25 dB of optical isolation and larger than 20 dB of isolation over 40 nm of tuning is fabricated and characterized. The device is carefully designed with laser integration in mind, and can be integrated with the heterogeneous silicon/III-V actives shown in Fig. 7 to realize the next generation of silicon based PIC.

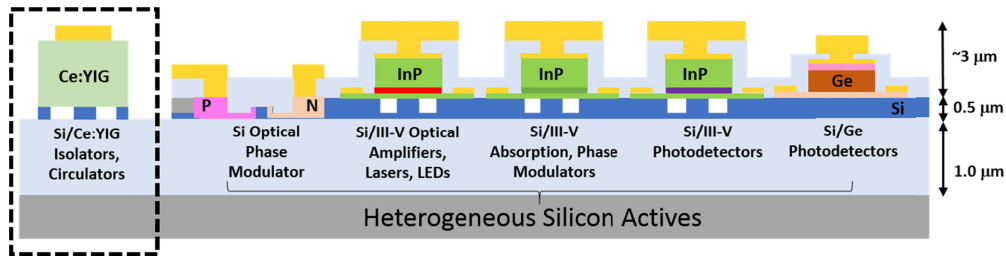


Fig. 7. The library of heterogeneous silicon/III-V components, with the addition of isolators and circulators.

Funding

Morton Photonics; Air Force SBIR (#FA8650-16-C-1758).

Acknowledgments

The authors acknowledge support of Morton Photonics and Air Force SBIR contract #FA8650-16-C-1758. The authors thank Tetsuya Mizumoto and Yuya Shoji for providing the Ce:YIG material, Jonathan Peters for fabrication assistance, as well as Paul Morton, Daoxin Dai, Minh Tran, and Tin Komljenovic for helpful discussions.

References and links

1. D. Thomson, A. Zilkie, J. E. Bowers, T. Komljenovic, G. T. Reed, L. Vivien, D. Marris-Morini, E. Cassan, L. Viroat, J. M. Fédéli, J. M. Hartmann, J. H. Schmid, D. X. Xu, F. Boeuf, P. O'Brien, G. Z. Mashanovich, and M. Nedeljkovic, "Roadmap on silicon photonics," *J. Opt.* **18**(7), 1–20 (2016).
2. J. Sun, E. Timurdogan, A. Yaacobi, E. S. Hosseini, and M. R. Watts, "Large-scale nanophotonic phased array," *Nature* **493**(7431), 195–199 (2013).
3. S. Miller, C. Phare, Y. Chang, X. Ji, O. J. Gordillo, S. R. A. Mohanty, M. Shin, B. Stern, M. Zadka, and M. Lipson, "512-Element Actively Steered Silicon Phased Array for Low-Power LIDAR," *Conf. Lasers Electro-Optics, JTh5C.2* (2018).
4. C. Sun, M. T. Wade, Y. Lee, J. S. Orcutt, L. Alloatti, M. S. Georgas, A. S. Waterman, J. M. Shainline, R. R. Avizienis, S. Lin, B. R. Moss, R. Kumar, F. Pavanello, A. H. Atabaki, H. M. Cook, A. J. Ou, J. C. Leu, Y. H. Chen, K. Asanović, R. J. Ram, M. A. Popović, and V. M. Stojanović, "Single-chip microprocessor that communicates directly using light," *Nature* **528**(7583), 534–538 (2015).
5. A. H. Atabaki, S. Moazeni, F. Pavanello, H. Gevorgyan, J. Notaros, L. Alloatti, M. T. Wade, C. Sun, S. A. Kruger, H. Meng, K. Al Qubaisi, I. Wang, B. Zhang, A. Khilo, C. V. Baiocco, M. A. Popović, V. M. Stojanović, and R. J. Ram, "Integrating photonics with silicon nanoelectronics for the next generation of systems on a chip," *Nature* **556**(7701), 349–354 (2018).
6. J. Wang, S. Paesani, Y. Ding, R. Santagati, P. Skrzypczyk, A. Salavrakos, J. Tura, R. Augusiak, L. Mančinska, D. Bacco, D. Bonneau, J. W. Silverstone, Q. Gong, A. Acin, K. Rottwitz, L. K. Oxenlöwe, J. L. O'Brien, A. Laing, M. G. Thompson, and M. G. Thompson, "Multidimensional quantum entanglement with large-scale integrated optics," *Science* **360**(6386), 285–291 (2018).
7. Z. Zhou, B. Yin, and J. Michel, "On-chip light sources for silicon photonics," *Light Sci. Appl.* **4**(11), 1–13 (2015).
8. D. Liang and J. E. Bowers, "Recent progress in lasers on silicon," *Nat. Photonics* **4**(8), 511–517 (2010).
9. D. Liang, G. Roelkens, R. Baets, and J. E. Bowers, "Hybrid integrated platforms for silicon photonics," *Materials (Basel)* **3**(3), 1782–1802 (2010).

10. B. Song, C. Stagarescu, S. Ristic, A. Behfar, and J. Klamkin, "3D integrated hybrid silicon laser," *Opt. Express* **24**(10), 10435–10444 (2016).
11. A. W. Fang, H. Park, O. Cohen, R. Jones, M. J. Paniccia, and J. E. Bowers, "Electrically pumped hybrid AlGaInAs-silicon evanescent laser," *Opt. Express* **14**(20), 9203–9210 (2006).
12. J. C. Hulme, J. K. Doylend, M. J. R. Heck, J. D. Peters, M. L. Davenport, J. T. Bovington, L. A. Coldren, and J. E. Bowers, "Fully integrated hybrid silicon two dimensional beam scanner," *Opt. Express* **23**(5), 5861–5874 (2015).
13. C. Zhang, S. Zhang, J. D. Peters, and J. E. Bowers, " $8 \times 8 \times 40$ Gbps fully integrated silicon photonic network on chip," *Optica* **3**(7), 785 (2016).
14. M. A. Tran, T. Komljenovic, J. C. Hulme, M. J. Kennedy, D. J. Blumenthal, and J. E. Bowers, "Integrated optical driver for interferometric optical gyroscopes," *Opt. Express* **25**(4), 3826–3840 (2017).
15. T. Komljenovic, M. Davenport, J. Hulme, A. Liu, C. Santis, A. Spott, S. Srinivasan, E. Stanton, C. Zhang, and J. Bowers, "Heterogeneous Silicon Photonic Integrated Circuits," *J. Lightwave Technol.* **34**, 1(2015).
16. Intel Corporation, "Intel Silicon Photonics," <https://www.intel.com/content/www/us/en/architecture-and-technology/silicon-photonics/silicon-photonics-overview.html>.
17. P. Pintus, N. Andrioli, F. Di Pasquale, and J. E. Bowers, "Bidirectional crosstalk and back-reflection free WDM active optical interconnects," *IEEE Photonics Technol. Lett.* **25**(20), 1973–1976 (2013).
18. D. Jalas, A. Petrov, M. Eich, W. Freude, S. Fan, Z. Yu, R. Baets, M. Popović, A. Melloni, J. D. Joannopoulos, M. Vanwolleghem, C. R. Doerr, and H. Renner, "What is-and what is not-an optical isolator," *Nat. Photonics* **7**(8), 579–582 (2013).
19. H. Lira, Z. Yu, S. Fan, and M. Lipson, "Electrically driven nonreciprocity induced by interband photonic transition on a silicon chip," *Phys. Rev. Lett.* **109**(3), 033901 (2012).
20. D. B. Sohn, S. Kim, and G. Bahl, "Time-reversal symmetry breaking with acoustic pumping of nanophotonic circuits," *Nat. Photonics* **12**(2), 91–97 (2018).
21. Z. Yu and S. Fan, "Complete optical isolation created by indirect interband photonic transitions," *Nat. Photonics* **3**(2), 91–94 (2009).
22. S. Bhandare, S. K. Ibrahim, D. Sandel, H. Zhang, F. Wüst, and R. Noé, "Novel nonmagnetic 30-dB traveling-wave single-sideband optical isolator integrated in III/V material," *IEEE J. Sel. Top. Quantum Electron.* **11**(2), 417–421 (2005).
23. C. R. Doerr, N. Dupuis, and L. Zhang, "Optical isolator using two tandem phase modulators," *Opt. Lett.* **36**(21), 4293–4295 (2011).
24. C. R. Doerr, L. Chen, and D. Vermeulen, "Silicon photonics broadband modulation-based isolator," *Opt. Express* **22**(4), 4493–4498 (2014).
25. Y. Shi, Z. Yu, and S. Fan, "Limitations of nonlinear optical isolators due to dynamic reciprocity," *Nat. Photonics* **9**(6), 388–392 (2015).
26. M. Krause, H. Rentier, and E. Brinkmeyer, "Optical isolation in silicon waveguides based on nonreciprocal Raman amplification," *Electron. Lett.* **44**(11), 691 (2008).
27. C. H. Dong, Z. Shen, C. L. Zou, Y. L. Zhang, W. Fu, and G. C. Guo, "Brillouin-scattering-induced transparency and non-reciprocal light storage," *Nat. Commun.* **6**(1), 6193 (2015).
28. S. Hua, J. Wen, X. Jiang, Q. Hua, L. Jiang, and M. Xiao, "Demonstration of a chip-based optical isolator with parametric amplification," *Nat. Commun.* **7**, 13657 (2016).
29. M. Levy, "The on-chip integration of magneto-optic waveguide isolators," *IEEE J. Sel. Top. Quantum Electron.* **8**(6), 1300–1306 (2002).
30. T. R. Zaman, X. Guo, and R. J. Ram, "Semiconductor waveguide isolators," *J. Lightwave Technol.* **26**(2), 291–301 (2008).
31. C. Zhang, P. Dulal, B. J. H. Stadler, and D. C. Hutchings, "Monolithically-Integrated TE-mode 1D Silicon-on-Insulator Isolators using Seedlayer-Free Garnet," *Sci. Rep.* **7**(1), 5820 (2017).
32. P. K. Tien, R. J. Martin, R. Wolfe, R. C. Le Craw, and S. L. Blank, "Switching and modulation of light in magneto-optic waveguides of garnet films," *Appl. Phys. Lett.* **21**(8), 394–396 (1972).
33. D. C. Hutchings and B. M. Holmes, "A waveguide polarization toolset design based on mode beating," *IEEE Photonics J.* **3**(3), 450–461 (2011).
34. H. Shimizu and Y. Nakano, "Fabrication and Characterization of an InGaAsp / InP Active Waveguide Optical Isolator With 14.7 dB / mm TE Mode Nonreciprocal Attenuation," *J. Lightwave Technol.* **24**(1), 38–43 (2006).
35. W. Van Parys, B. Moeyersoon, D. Van Thourhout, R. Baets, M. Vanwolleghem, B. Dagens, J. Decobert, O. Le Gouezigou, D. Make, R. Vanheertum, and L. Lagae, "Transverse magnetic mode nonreciprocal propagation in an amplifying AlGaInAs/InP optical waveguide isolator," *Appl. Phys. Lett.* **88**(7), 071115 (2006).
36. H. Shimizu and Y. Nakano, "Monolithic integration of a waveguide optical isolator with a distributed feedback laser diode in the 1.5- μ m wavelength range," *Technology* **19**, 1973–1975 (2007).
37. N. Kono, K. Kakihara, K. Saitoh, and M. Koshiba, "Nonreciprocal microresonators for the miniaturization of optical waveguide isolators," *Opt. Express* **15**(12), 7737–7751 (2007).
38. M.-C. Tien, T. Mizumoto, P. Pintus, H. Kromer, and J. E. Bowers, "Silicon ring isolators with bonded nonreciprocal magneto-optic garnets," *Opt. Express* **19**(12), 11740–11745 (2011).
39. L. Bi, J. Hu, P. Jiang, D. H. Kim, G. F. Dionne, L. C. Kimerling, and C. A. Ross, "On-chip optical isolation in monolithically integrated non-reciprocal optical resonators," *Nat. Photonics* **5**(12), 758–762 (2011).
40. D. Huang, P. Pintus, C. Zhang, Y. Shoji, T. Mizumoto, and J. E. Bowers, "Electrically driven and thermally

- tunable integrated optical isolators for silicon photonics,” *IEEE J. Sel. Top. Quantum Electron.* **22**(6), 271–278 (2016).
41. Y. Shoji, T. Mizumoto, H. Yokoi, I. W. Hsieh, and R. M. Osgood, Jr., “Magneto-optical isolator with silicon waveguides fabricated by direct bonding,” *Appl. Phys. Lett.* **92**(7), 071117 (2008).
 42. J. Fujita, M. Levy, R. M. Osgood, Jr., L. Wilkens, and H. Dötsch, “Waveguide optical isolator based on Mach-Zehnder interferometer,” *Appl. Phys. Lett.* **76**(16), 2158–2160 (2000).
 43. J. S. Yang, J. W. Roh, S. H. Ok, D. H. Woo, Y. T. Byun, W. Y. Lee, T. Mizumoto, and S. Lee, “An integrated optical waveguide isolator based on multimode interference by wafer direct bonding,” *IEEE Trans. Magn.* **41**(10), 3520–3522 (2005).
 44. Z. Wang and S. Fan, “Optical circulators in two-dimensional magneto-optical photonic crystals,” *Opt. Lett.* **30**(15), 1989–1991 (2005).
 45. Y. Shoji, K. Miura, and T. Mizumoto, “Optical nonreciprocal devices based on magneto-optical phase shift in silicon photonics,” *J. Opt.* **18**, 1 (2015).
 46. D. Huang, P. Pintus, Y. Shoji, P. Morton, T. Mizumoto, and J. E. Bowers, “Integrated broadband Ce:YIG/Si Mach-Zehnder optical isolators with over 100 nm tuning range,” *Opt. Lett.* **42**(23), 4901–4904 (2017).
 47. P. Pintus, F. Di Pasquale, and J. E. Bowers, “Integrated TE and TM optical circulators on ultra-low-loss silicon nitride platform,” *Opt. Express* **21**(4), 5041–5052 (2013).
 48. A. D. Block, P. Dulal, B. J. H. Stadler, and N. C. A. Seaton, “Growth parameters of fully crystallized YIG, Bi:YIG, and Ce:YIG films with high Faraday rotations,” *IEEE Photonics J.* **6**(1), 1–8 (2014).
 49. M. C. Onbasli, L. Beran, M. Zahradnik, M. Kučera, R. Antoš, J. Mistrík, G. F. Dionne, M. Veis, and C. A. Ross, “Optical and magneto-optical behavior of cerium yttrium iron garnet thin films at wavelengths of 200–1770 nm,” *Sci. Rep.* **6**(1), 23640 (2016).
 50. K. Srinivasan, T. E. Gage, and B. J. H. Stadler, “Seed-layer free cerium-doped terbium iron garnet on non-garnet substrates for photonic isolators,” in *Conference on Lasers and Electro-Optics*, OSA Technical Digest (online) (Optical Society of America, 2018), paper SW4I.5 (2018).
 51. T. Shintaku, “Integrated optical isolator based on efficient nonreciprocal radiation mode conversion,” *Appl. Phys. Lett.* **73**(14), 1946–1948 (1998).
 52. T. Mizumoto, R. Baets, and J. E. Bowers, “Optical nonreciprocal devices for silicon photonics using wafer-bonded magneto-optical garnet materials,” *MRS Bull.* **43**(6), 419–424 (2018).
 53. M. Davenport, “Heterogeneous silicon III-V mode-locked lasers,” *Photon. Res.* **6**, 468–478 (2018).
 54. T. Goto, M. C. Onbaşlı, and C. A. Ross, “Magneto-optical properties of cerium substituted yttrium iron garnet films with reduced thermal budget for monolithic photonic integrated circuits,” *Opt. Express* **20**(27), 28507–28517 (2012).
 55. P. Dulal, A. D. Block, T. E. Gage, H. A. Haldren, S. Y. Sung, D. C. Hutchings, and B. J. H. Stadler, “Optimized magneto-optical isolator designs inspired by seedlayer-free terbium iron garnets with opposite chirality,” *ACS Photonics* **3**(10), 1818–1825 (2016).
 56. P. Dong, T.-C. Hu, T.-Y. Liow, Y.-K. Chen, C. Xie, X. Luo, G.-Q. Lo, R. Kopf, and A. Tate, “Novel integration technique for silicon/III-V hybrid laser,” *Opt. Express* **22**(22), 26854–26861 (2014).
 57. S. Keyvaninia, G. Roelkens, D. Van Thourhout, C. Jany, M. Lamponi, A. Le Liepvre, F. Lelarge, D. Make, G.-H. Duan, D. Bordel, and J.-M. Fedeli, “Demonstration of a heterogeneously integrated III-V/SOI single wavelength tunable laser,” *Opt. Express* **21**(3), 3784–3792 (2013).
 58. P. Pintus, “Accurate vectorial finite element mode solver for magneto-optic and anisotropic waveguides,” *Opt. Express* **22**(13), 15737–15756 (2014).
 59. G. Beaudin, A. Belarouci, and V. Aimez, “Precise localized thinning and vertical taper fabrication for silicon photonics using a modified local oxidation of silicon (LOCOS) fabrication process,” *Opt. Express* **23**(4), 4377–4384 (2015).
 60. E. Ishida, K. Miura, Y. Shoji, H. Yokoi, T. Mizumoto, N. Nishiyama, and S. Arai, “Amorphous-Si waveguide on a garnet magneto-optical isolator with a TE mode nonreciprocal phase shift,” *Opt. Express* **25**(1), 452–462 (2017).
 61. P. Pintus, F. Di Pasquale, and J. E. Bowers, “Design of transverse electric ring isolators for ultra-low-loss Si₃N₄ waveguides based on the finite element method,” *Opt. Lett.* **36**(23), 4599–4601 (2011).
 62. S. Ghosh, S. Keyvaninia, Y. Shirato, T. Mizumoto, G. Roelkens, and R. Baets, “Optical isolator for TE polarized light realized by adhesive bonding of Ce:YIG on silicon-on-insulator waveguide circuits,” *IEEE Photonics J.* **5**(3), 6601108 (2013).
 63. Y. Shoji, A. Fujie, and T. Mizumoto, “Silicon waveguide optical isolator operating for TE mode input light,” *IEEE J. Sel. Top. Quantum Electron.* **22**(6), 264–270 (2016).
 64. D. Dai, L. Liu, S. Gao, D.-X. Xu, and S. He, “Polarization management for silicon photonic integrated circuits,” *Laser Photonics Rev.* **7**(3), 303–328 (2013).
 65. D. Dai, J. Bauters, and J. E. Bowers, “Passive technologies for future large-scale photonic integrated circuits on silicon: Polarization handling, light non-reciprocity and loss reduction,” *Light Sci. Appl.* **1**(3), 1–12 (2012).
 66. D. Dai and J. E. Bowers, “Novel concept for ultracompact polarization splitter-rotator based on silicon nanowires,” *Opt. Express* **19**(11), 10940–10949 (2011).
 67. J. Leuthold, J. Eckner, J. Eckner, and E. Gamper, “Multimode interference couplers for the conversion and combining of 0th & 1st-order modes,” *J. Lightwave Technol.* **16**, 1228–1239 (1998).
 68. W. D. Sacher, T. Barwicz, B. J. F. Taylor, and J. K. S. Poon, “Polarization rotator-splitters in standard active

- silicon photonics platforms,” *Opt. Express* **22**(4), 3777–3786 (2014).
69. R. R. Abbott, V. J. Fratello, S. J. Licht, and I. Mnushkina, “Article comprising a Faraday rotator that does not require a bias magnet,” U.S. patent 6770223 B1 (August 3, 2004).
 70. D. Karki, V. Stenger, A. Pollick, and M. Levy, “Thin-film magnetless Faraday rotators for compact heterogeneous integrated optical isolators,” *J. Appl. Phys.* **121**(23), 233101 (2017).
 71. P. Pintus, D. Huang, C. Zhang, Y. Shoji, T. Mizumoto, and J. E. Bowers, “Microring-based optical isolator and circulator with integrated electromagnet for silicon photonics,” *J. Lightwave Technol.* **35**(8), 1429–1437 (2017).
 72. J. R. Black, “Electromigration—A brief survey and some recent results,” *Electron Devices, IEEE Trans.* **16**(4), 338–347 (1969).
 73. M. Bruel, “The history, physics, and applications of the smart-cut process,” *MRS Bull.* **23**(12), 35–39 (1998).
 74. M. Levy, R. M. Osgood, Jr., A. Kumar, and H. Bakhru, “Crystal ion slicing of single-crystal magnetic garnet films,” *J. Appl. Phys.* **83**(11), 6759–6761 (1998).
 75. S. Ghosh, S. Keyvavinia, W. Van Roy, T. Mizumoto, G. Roelkens, and R. Baets, “Ce:YIG/Silicon-on-Insulator waveguide optical isolator realized by adhesive bonding,” *Opt. Express* **20**(2), 1839–1848 (2012).
 76. M. Levy, R. M. Osgood, H. Hegde, F. J. Cadieu, R. Wolfe, and V. J. Fratello, “Integrated optical isolators with sputter-deposited thin-film magnets,” *IEEE Photonics Technol. Lett.* **8**(7), 903–905 (1996).
 77. K. Okazeri, K. Muraoka, Y. Shoji, S. Nakagawa, N. Nishiyama, S. Arai, and T. Mizumoto, “Self-Holding Magneto-Optical Switch Integrated with Thin-Film Magnet,” *IEEE Photonics Technol. Lett.* **30**(4), 371–374 (2018).
 78. P. Dong, A. Melikyan, and K. Kim, “Commercializing Silicon Microring Resonators : Technical Challenges and Potential Solutions,” in *CLEO* (2018), pp. 5–6.